Journal of Medicinal Chemistry

Article

pubs.acs.org/jmc

Structure-Based Design of Potent and Ligand-Efficient Inhibitors of CTX-M Class A β-Lactamase

Derek A. Nichols,[†] Priyadarshini Jaishankar,[‡] Wayne Larson,[‡,∥] Emmanuel Smith,[†] Guoqing Liu,[†] Racha Beyrouthy,[§,⊥] Richard Bonnet,[§] Adam R. Renslo,*[,‡] and Yu Chen*[,†]

[†]University of South Florida College of Medicine, Department of Molecular Medicine,12901 Bruce B. Downs Boulevard, MDC 3522, Tampa, Florida 33612, United States

[‡]Department of Pharmaceutical Chemistry and Small Molecule Discovery Center, University of California San Francisco, 1700 Fourth Street, Byers Hall S504, San Francisco, California 94158, United States

[§]Clermont Université, Université d'Auvergne, M2iSH, BP10448, INRA, USC 2018, CHU Clermont-Ferrand, Service de Bactériologie, F-63003 Clermont-Ferrand, France

ABSTRACT: The emergence of CTX-M class A extended-spectrum β-lactamases poses a serious health threat to the public. We have applied structure-based design to improve the potency of a novel noncovalent tetrazole-containing CTX-M inhibitor (K_i = 21 μM) more than 200-fold via structural modifications targeting two binding hot spots, a hydrophobic shelf formed by Pro167 and a polar site anchored by Asp240. Functional groups contacting each binding hot spot independently in initial designs were later combined to produce analogues with submicromolar potencies, including 6-trifluoromethyl-3*H*-benzoimidazole-4-carboxylic acid [3-(1*H*-tetrazol-5-yl)-phenyl]-amide, which had a K_i value of 89 nM and reduced the MIC of cefotaxime by 64-fold in CTX-M-9 expressing *Escherichia coli*. The in vitro potency gains were accompanied by improvements in ligand efficiency (from 0.30 to 0.39) and LipE (from 1.37 to 3.86). These new analogues represent the first nM-affinity noncovalent inhibitors of a class A β-lactamase. Their complex crystal structures provide valuable information about ligand binding for future inhibitor design.

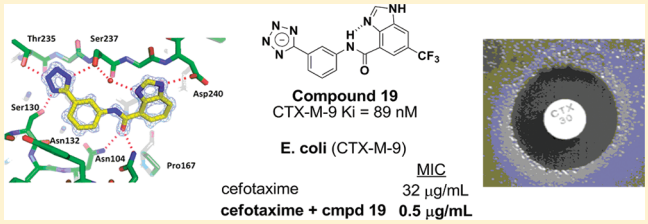

INTRODUCTION

β-Lactam compounds, such as penicillins, are the most widely used antibiotics due to their effective inhibition of the transpeptidases required for bacterial cell wall synthesis.[1−4] β-Lactamases catalyze β-lactam hydrolysis and are primary mediators of bacterial resistance to these compounds.[5−7] There are four β-lactamase families, classes A−D, among which classes A and C are the most commonly observed in the clinic.[8,9] CTX-M is a new group of class A β-lactamases that is particularly effective against the extended spectrum β-lactam antibiotics such as cefotaxime,[10−14] which itself was developed to counter bacterial resistance to first-generation penicillins and cephalosporins. The widespread emergence of extended spectrum β-lactamase (ESBL) such as CTX-M will continue to limit treatment options for bacterial infections. Since its discovery in the 1990s, CTX-M has become the most frequently observed ESBL in many regions of the world.

The use of a β-lactamase inhibitor in combination with a β-lactam antibiotic is a well-established strategy to counter resistance.[15] Existing β-lactamase inhibitors (e.g., clavulanic acid) generally contain a β-lactam ring, making them susceptible to resistance stemming from up-regulation of β-lactamase production, selection for new β-lactamases, and other mechanisms evolved over millions of years of chemical warfare between bacteria and β-lactam producing microorganisms.[16−19] In principle, these problems can be overcome by developing structurally novel (non-β-lactam) inhibitors of β-lactamases.[20−24]

We recently described our application of fragment-based molecular docking to identify a new class of noncovalent inhibitors of CTX-M β-lactamase.[25,26] The fragment-based approach allowed us to overcome the limited chemical diversity of lead/drug-sized compound libraries, which presents a particularly challenging problem for antibiotic discovery. This is due to the starkly different chemical features of antibiotics when compared to drugs targeting human proteins such as GPCRs, toward which most HTS screening libraries are inherently biased.[27−29] Thus, our virtual screening of fragment libraries led to the discovery of a tetrazole-based inhibitor chemotype, represented by compound **1**, at the time the highest affinity (K_i = 21 μM) noncovalent inhibitor of any class A β-lactamase (Figure 1, Table 1). The tetrazole-based chemotype appealed to us for several reasons. First, the tetrazole group has excellent shape and electrostatic complementarity with the active site subpocket of CTX-M that usually binds the C(3)4′ carboxylate of traditional β-lactam antibiotics (Figure 1). Second, the tetrazole ring is a well-known binding bioisostere for carboxylate groups that often possesses more favorable pharmacokinetic properties.

Received: October 19, 2011
Published: February 1, 2012

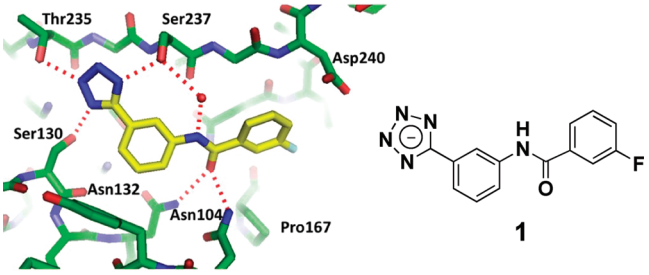

Figure 1. Crystal structure of compound **1** in complex with CTX-M-9.[25] Compound **1** (K_i = 21 μM) carbon atoms are shown in yellow, nitrogens in blue, oxygens in red, and fluorine in light blue. The dashed lines represent hydrogen bonds with a sphere representing a water molecule.

Close examination of the complex crystal structure with compound **1** revealed two potential binding hot spots that might be exploited to improve affinity (Figure 1). The first is a relatively nonpolar binding surface surrounding Pro167, while the second site, anchored by Asp240, suggested the possibility of introducing a favorable electrostatic interaction. The design and synthesis of compounds that focused on interacting with these binding hot spots has resulted in several novel high affinity noncovalent inhibitors. The binding of many new inhibitors to the CTX-M active site was further investigated using X-ray crystallography. Targeting both hot spots with small substituents allowed us to identify more ligand-efficient inhibitors, including the highest affinity (K_i = 89 nM) noncovalent inhibitor of a class A β-lactamase reported to date.

RESULTS

Structure-Based Design. Compound **1** and other less potent inhibitors were identified by a molecular docking screen of the ZINC lead-like database using the program DOCK.[25,30−32] In the complex crystal structure of **1** with CTX-M, the fluoro-benzene ring is in close proximity to Asp240 and the binding surface surrounding Pro167. Two carbon atoms on the fluoro-benzene ring are in vdw contact (3.43 Å) with the Oδ1 atom of Asp240. Although there are favorable electrostatic interactions between the ring hydrogen atoms of **1** and Asp240 Oδ1, we hypothesized that a hydrogen bonding interaction or a salt bridge to Asp240 in a modified ligand would greatly enhance binding affinity. In a previously determined complex structure with a boronic acid inhibitor bearing a ceftazidime side chain (PDB ID 1YLY),[12] Asp240 has been observed to form such a hydrogen bond with the ligand's distal amine group, which may partially account for the improved β-lactamase activity of CTX-M against ceftazidime. Meanwhile, the fluorine atom of compound **1** is 4−5 Å away from a cluster of protein carbon atoms including Pro167Cβ, Pro167Cγ, Pro167C, Thr168Cα, and Thr171Cγ, suggesting that more favorable vdw contacts and hydrophobic interactions could be formed between this site and analogues modified at the three position of the aryl ring. Hence, on the basis of these observations from the complex structure of **1**, two series of analogues independently targeting each of the two potential binding hot spots were designed, docked, and synthesized.

Synthesis. The simple achiral structure of **1** is an attractive feature of this chemotype compared to traditional β-lactamase inhibitors. Designed analogues that docked well to CTX-M computationally were synthesized in 1−3 synthetic steps or in some cases could be purchased commercially. Thus, reaction of commercially available 3-(1*H*-tetrazol-5-yl)aniline with various commercial or synthesized carboxylic acids or acid chlorides afforded the final analogues. Our initial designs focused exclusively on the 3-fluoro aryl ring of **1** as this moiety is in proximity to both of the putative binding hot spots we sought to target. The aryl tetrazole moiety of **1** appears to be highly complementary to its binding site already and was thus viewed as a structural anchor that would be unlikely to bind much differently in the new analogues. This prediction was borne out when complex structures of new analogues were solved, as detailed later.

Enzymology and Binding Affinities. To investigate the effectiveness of the new analogues, we employed CTX-M-9 and a UV-absorbance based biochemical assay to obtain binding affinities. A series of analogues with modifications at the three position were evaluated with the expectation that these compounds would form more favorable nonpolar contacts with Pro167 (Table 1). Compounds **2**−**11** possess 3-substituents of roughly increasing size and with generally lipophilic character, though not exclusively so. Interestingly, all of these modified analogues proved superior to **1** in terms of K_i,

Table 1. Analogues Designed to Target Hydrophobic Shelf Formed by Pro167

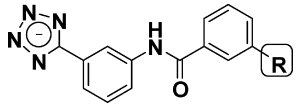

compd	R =	K_i (μM)	LE[a]	LipE[b]
1	F	21	0.30	1.37
2	Cl	6.2	0.34	1.63
3	Me	4.5	0.35	1.84
4	Br	3.0	0.36	1.74
5	cyclopropyl	3.1	0.33	1.74
6	OMe	17.1	0.30	1.95
7	Ac	10.2	0.30	2.51
8	NO_2	3.8	0.32	2.45
9	CO_2Me	6.9	0.29	2.09
10	CF_3	2.4	0.32	1.73
11	2-pyrimidyl	9.7	0.26	1.57

[a]LE, ligand efficiency; ΔG_{bind}(kcal)/(no. of heavy atoms). [b]LipE = pK_i − clogP (clogP calculated using MarvinSketch 5.5.0.1).

dx.doi.org/10.1021/jm2014138 | J. Med. Chem. 2012, 55, 2163−2172

but the most ligand-efficient analogues were those possessing spheroid hydrophobes (e.g., Me, Br, CF_3). The highest affinity compound from the series targeting Pro167 was compound **10**, the 3-trifluoromethyl variant, with a K_i of 2.4 μM (Table 1). Analogues **6**–**8**, bearing less hydrophobic and nonspheroid substituents, had similar ligand efficiency as **1** but superior LipE values (1.37 for **1** vs 2.51 for **7**). The parameter LipE (defined as logK_i − clogP)[33] provides a measure of binding affinity improvement achieved while retaining favorable physiochemical properties. A surprising result was that even large substituents (2-pyrimidyl, compound **11**) could be tolerated at the 3-position, although ligand efficiency suffers. A complex crystal structure of **11** confirmed a similar binding pose as **1** (see below), so the reduced ligand efficiency of this analogue perhaps reflects a steric clash and/or unfavorable desolvation energy associated with the burial of a pyrimidine ring nitrogen atom.

To target the second hot spot comprising the area around Asp240, we designed analogues bearing hydrogen bond donors and/or charged side chains at various positions on the aryl ring. These various designs were docked to CTX-M and some of the best-scoring analogues were synthesized and tested in the biochemical assay (Table 2). Our attempt to form a salt bridge

Table 2. Analogues Designed to Target Asp240

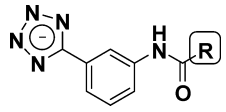

Compound	R =	K_i (μM)	L.E.[a]	LipE[b]
12		76.0	0.23	2.22
13	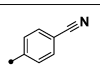	no inhibition	N/A	N/A
14		7.2	0.32	2.27
15		6.6	0.31	2.05
16		1.3	0.35	3.58
17		1.9	0.34	2.59
18		1.1	0.35	3.55

[a]LE, ligand efficiency; ΔG_{bind}(kcal)/(no. of heavy atoms). [b]LipE = pK_i − clogP (clogP calculated using MarvinSketch 5.5.0.1).

to Asp240 by the introduction of a basic dimethylamino side chain (compound **12**) was unsuccessful, the analogue possessing only modest affinity (K_i = 76 μM). The regioisomeric aryl nitriles **13** and **14** had very different affinities, with meta-substitution as in **14** preferred (K_i = 7.2 μM). By far the most interesting analogues from this series (K_i ∼ 1 μM) were the heterocyclic analogues **16**–**18**, each of which possesses a potential hydrogen bond donor in a position (pseudo meta or para) predicted by docking to be in close proximity to Asp240. Moreover, compounds **16**–**18** exhibited improved ligand efficiency (0.34–0.35) and LipE values (2.59–3.58) as compared to **1** (0.31 and 1.37).

From these initial two libraries, we concluded that the independent targeting of each binding hot spot (Asp240 and Pro167) could indeed be leveraged to produce more potent and ligand-efficient inhibitors. As described below, the design principles and predicted binding poses of these initial analogues were validated by the solution of complex crystal structures for representative examples. Having identified more favorable binding elements for both hot spots, the logical next step was to combine these to produce inhibitors that targeted both sites simultaneously (Table 3). Indeed, the combination of a

Table 3. Analogues Designed to Target Both Pro167 and Asp240

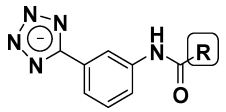

Compound	R =	K_i (μM)	L.E.[a]	LipE[b]
19	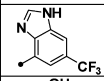	0.089	0.36	3.86
20		0.57	0.39	2.74
21		0.63	0.34	2.59
22		1.0	0.33	2.89
23		2.7	0.32	3.11
24		34.1	0.26	0.83

[a]LE, ligand efficiency; ΔG_{bind}(kcal)/(no. of heavy atoms). [b]LipE = pK_i − clogP (clogP calculated using MarvinSketch 5.5.0.1).

benzimidazole ring as in **16** with a trifluoromethyl substituent as in **10**, afforded analogue **19**, the most potent analogue yet identified (K_i = 89 nM; LE = 0.36; LipE = 3.86). We expected that the benzimidazole ring in **19** might contribute an important hydrogen bond to Asp240 and therefore explored whether simple hydroxyl or amino substituents in this position could function similarly (analogues **20**–**22**). These analogues were indeed more potent than the direct comparators **4** and **10** which lack a hydrogen bond donor but **20**–**22** were not as potent as **19**. As detailed later, the solution of a complex structure of benzimidazole analogue **16** revealed additional contacts that may explain the improved potency of benzimidazole **19** as compared to **20** and **22**. Unexpectedly, the fluoro benzimidazole analogue **23** was only equipotent to des-fluoro comparator **16**, the flouro substituent apparently not providing any additional affinity via putative interaction with Pro167. Perhaps tighter association of the benzimidazole ring with Asp240 draws the ligand slightly away from Pro167, thus requiring a larger substituent (such as trifluoromethyl in **19**) to productively contact Pro167.

X-ray Crystallographic Structure Determination. The structural details of the interactions between CTX-M-9 and several of the new analogues were investigated in order to gain an understanding of the molecular basis for the binding affinity improvement and to facilitate future inhibitor development. Complex crystal structures with CTX-M-9 were determined to

dx.doi.org/10.1021/jm2014138 | J. Med. Chem. 2012, 55, 2163–2172

Table 4. X-Ray Data Collection and Refinement Statistics

	compounds					
	4	**10**	**11**	**12**	**16**	**18**
Data Collection						
space group	$P2_1$	$P2_1$	$P2_1$	$P2_1$	$P2_1$	$P2_1$
cell dimensions						
a (Å)	45.174	45.014	45.245	45.125	45.192	45.166
b (Å)	107.188	107.105	106.941	106.922	106.565	106.567
c (Å)	47.487	47.509	47.681	47.481	47.669	47.825
α (deg)	90	90	90	90	90	90
β (deg)	100.38	102.105	100.972	101.469	101.717	101.857
γ (deg)	90	90	90	90	90	90
resolution (Å)	50−1.44	50−1.36	50−1.36	50−1.40	50−1.12	50−1.26
no. reflns	75901	92455	87996	86200	158174	118432
R_{merge} (%)	6.3	6.0	5.6	7.0	5.7	4.2
$I/\sigma I$	12.9(2.2)[a]	17.9(2.1)	18.2(2.1)	14.8(2.1)	14.7(3.0)	21.2(4.0)
completeness (%)	95.0	98.9	92.5	99.7	93.3	99.4
redundancy	2.5	3.7	3.7	3.7	3.6	3.7
Refinement						
resolution (Å)	50−1.44	50−1.36	50−1.36	50−1.40	50−1.12	50−1.26
R_{work}/R_{free} (%)	16.3/20.6	17.1/20.5	15.6/19.9	15.4/19.4	13.4/16.6	12.3/16.3
no. heavy atoms						
protein	4017	3941	3990	4023	4085	4090
ligand/ion	238	300	134	104	50	76
water	480	519	493	546	734	752
B factors (Å^2)						
protein	11.70	12.40	8.414	10.76	7.028	8.856
ligand/ion	24.84	22.90	19.73	14.42	6.883	14.70
water	27.64	28.08	24.47	26.58	21.29	23.78
rms deviations						
bond lengths (Å)	0.013	0.015	0.011	0.007	0.012	0.011
bond angles (deg)	1.555	1.656	1.380	1.149	1.482	1.437
Ramachandran plot						
most favored region (%)	96.9	97.2	96.7	96.6	96.7	96.7
additionally allowed (%)	1.9	1.8	2.1	2.3	2.0	2.0
generously allowed (%)	1.2	1.0	1.3	1.1	1.3	1.3

[a]Values in parentheses represent highest resolution shells.

a resolution in the range of 1.2−1.4 Å, where the ligand binding pose can be determined unambiguously. In all of these structures, the inhibitor adopts a single pose, as shown by the unbiased $F_o - F_c$ electron densities calculated prior to the fitting of the ligand (Table 4).

Figure 2 shows the X-ray crystal structures of compounds **4**, **10**, and **11** in the active site of CTX-M-9; these compounds were designed to make significant nonpolar interactions with Pro167. The size increase in the bulkier side substituents such as trifluoromethyl is demonstrated in their larger electron density volumes compared with that of the fluorine atom in **1**. In the larger sense, the atoms of the new ligands make similar contacts with the surrounding active site atoms, as does **1**. For instance, compounds **4**, **10**, and **11** (Figure 2a−c) all form hydrogen bonds between the tetrazole ring and Thr235, Ser237, and Ser130 from the protein, which is similar to compound **1** (Figure 1, Table 1). They also share the characteristic water-mediated interaction between the amide linkage and Ser237, as well as two hydrogen bonds with Asn132 or Asn104. The contacts between the distal benzene ring and Asp240, as observed in compound **1**, are maintained in compounds **4** and **10**, with two ring carbon atoms in vdw contact and approximately 3.2−3.3 Å away from the Oδ1 atom of Asp240. The favorable contacts between Pro167 and the functional groups on **4** and **10** are evident. The bromine atom on the ring structure of **4** is 4−5 Å away from the cluster of protein carbon atoms including Pro167Cβ, Pro167Cγ, Pro167C, Thr168Cα, and Thr171Cγ. Likewise, the three branched fluorine atoms of compound **10** are in close vdw contact with these protein carbon atoms, which are approximately 3.4−3.8 Å away. The binding of compound **11**, on the other hand, differs slightly from compounds **1**, **4**, and **10** in these regions (Figure 2c). The pyrimidine ring forms a water-mediated interaction with Asp240 and induces Asp240 to adopt a new conformation (Figure 2). This water-mediated contact exists in the complex structure with only partial occupancy, as suggested by the relatively weak electron density of the water (2σ) and the presence of two Asp240 conformations, including the one previously observed in apo and other complex structures. There is vdw contact observed between the carbon atoms of the pyrimidine ring in **11** and Pro167Cγ, Thr168Cγ, and Thr171Cγ, which are 3.3−3.6 Å away. Despite the water-mediated hydrogen bond and vdw contacts between the ring carbon atoms and Pro167 and Thr168, the affinity of compound **11** is less than that of **4** or **10**; this may be due to unfavorable burial of a polar pyrimidine ring nitrogen atom and electrostatic repulsion between this nitrogen and Pro167O. Additionally, the vdw contacts

dx.doi.org/10.1021/jm2014138 | J. Med. Chem. 2012, 55, 2163−2172

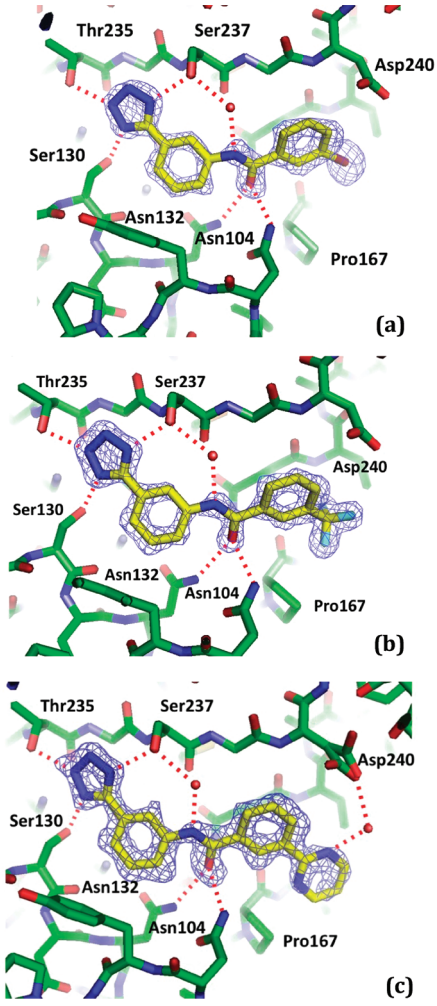

Figure 2. Crystal complex structures with compounds targeting Pro167. (a) Compound **4**. (b) Compound **10**. (c) Compound **11**. The red dashed lines represent hydrogen bonds between the ligand and CTX-M-9. The carbon atoms of the protein are colored in green along with oxygens in red and nitrogens in blue. The ligand carbon atoms are colored yellow. Resolution for the structures ranges from 1.2 to 1.4 Å. Unbiased $F_o - F_c$ densities are shown in blue at 3σ.

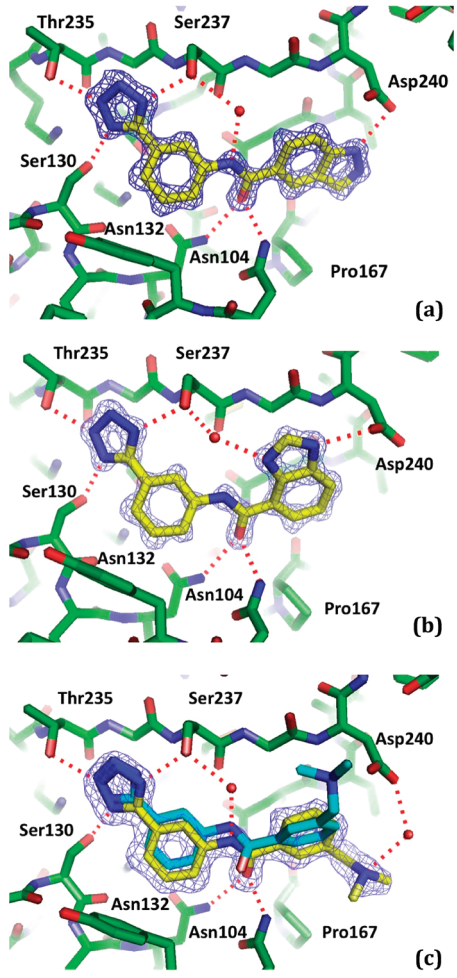

Figure 3. Crystal complex structures with compounds targeting Asp240. (a) Compound **18**. (b) Compound **16**. (c) Compound **12**, in comparison to the designed pose in cyan. The red dashed lines represent hydrogen bonds between the ligand and CTX-M-9. The carbon atoms of the protein are colored in green along with oxygens in red and nitrogens in blue. The ligand carbon atoms are colored yellow. Resolution for the structures ranges from 1.2 to 1.4 Å. Unbiased $F_o - F_c$ densities are shown in blue at 3σ.

described above may be slightly too close for the optimal carbon−carbon distance in vdw interaction (~4 Å) and thus suggest a possible minor steric clash.

Crystal structures were also obtained for compounds designed to establish polar interactions with Asp240, including compounds **12**, **16**, and **18**. Again, the core structure of these compounds, including the tetrazole ring and the amide bond, establishes contacts with Ser130, Thr235, Ser237, Asn104, and Asn132, similar to compound **1** (Figure 3a−c). Both compounds **16** and **18** form a direct hydrogen bond with Asp240 as designed. In addition, compound **16** has a favorable contact between N-1/C-2/N-3 of the benzimidazole ring and the main chain atoms around Gly238, while compound **18** establishes more vdw interactions with Pro167 and Thr168. The second ring nitrogen (N-3) in benzimidazole **16**, which is a carbon in indole **15**, appears to form a water-mediated hydrogen bonding contact with Ser237 (Figure 3b). However, the electron density for the water molecule contacting N-3 in **16** is weaker (2.4σ) than other structural waters in the active site, suggesting that this water-mediated interaction is relatively unstable and may not contribute to binding affinity significantly. The modest additional affinity of compound **16**, in comparison to **15**, may instead originate from an intramolecular hydrogen bond between N-3 and the proximal amide N−H, an interaction that would stabilize the conformation conducive to hydrogen bond formation with Asp240.

Figure 3c shows the discrepancy between the designed interaction of compound **12** with Asp240 (in cyan) and its actual interactions observed in the crystal structure (in yellow). Initially, we designed compound **12** to form a salt bridge with Asp240. However, the X-ray crystal structure reveals the actual binding pose in which a water-mediated hydrogen bond is formed between the positively charged side chain and Asp240. The new side chain is cradled in the small pocket surrounding Pro167, once again underscoring the potential of this binding surface in establishing new interactions with future inhibitors.

Antimicrobial Activity. The activity of compound **19** was investigated in clinical bacterial isolates that exhibit high levels of resistance against third-generation cephalosporins (e.g., cefotaxime) via expression of CTX-M β-lactamases. When the compound was administrated alone in a disk diffusion assay, it

dx.doi.org/10.1021/jm2014138 | J. Med. Chem. 2012, 55, 2163−2172

had little or no detectable effect on bacteria growth, as expected (Figure 4). However, in combination with cefotaxime, the

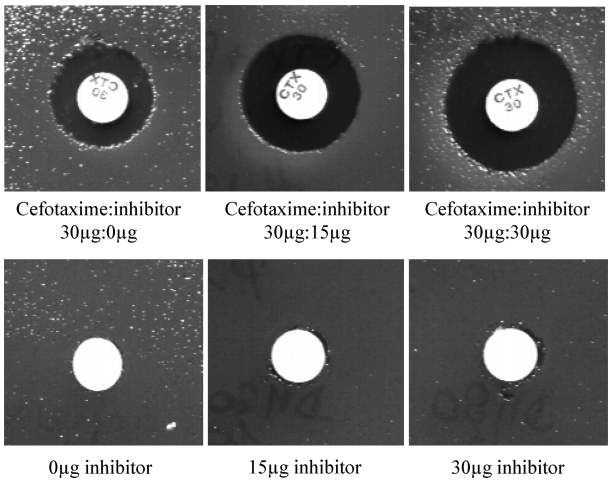

Figure 4. Disk diffusion plate assay showing the antimicrobial activity of compound **19**. The compound was administered alone or in combination with cefotaxime against an *E. coli* strain producing CTX-M-9 β-lactamase.

compound produced a large inhibition halo surrounding the disk. The size of the inhibition zone showed improved inhibition of bacterial growth compared to cefotaxime alone and increased with the concentration of the compound. This dose-responsive inhibition of bacterial growth revealed clear synergy between cefotaxime and **19**.

Antimicrobial activity was investigated quantitatively to determine the minimum inhibitory concentrations (MICs) of the β-lactam/inhibitor combination necessary to inhibit bacterial growth. The MICs of cefotaxime alone against the two *Escherichia coli* strains, expressing CTX-M-14 and CTX-M-9, respectively, corresponded to a high level of resistance (MICs, 32 and 64 μg/mL) according to Clinical and Laboratory Standards Institute (CLSI) standards.[34] Compound **19** had no measurable antibiotic activity when used alone (MIC $\geq$ 64 μg/mL). In combination with cefotaxime, compound **19** improved MIC values by 64-fold and restored susceptibility to cefotaxime in these resistant bacterial strains (MICs, 0.5 and 1 μg/mL). These results provide evidence that compound **19** is able to cross bacterial outer membrane to access its intended target.

DISCUSSION

The identification of novel noncovalent inhibitors of class A β-lactamases is a promising approach to maintain the effectiveness of β-lactam antibiotics. The purpose of this initial study was to rapidly identify regions of the active site that could be more productively engaged with designed ligands, thus enabling further optimization of tetrazole-based inhibitors of CTX-M β-lactamase. The targeted introduction of new functional groups in the distal ring of **1** succeeded in producing improved analogues that make both nonpolar and polar contacts with CTX-M β-lactamase, improving affinity ~200-fold while retaining good lead-like properties (reflected in notably improved LipE values). The results confirm the importance of Pro167 and Asp240 as binding hot spots in CTX-M β-lactamase and demonstrate the tractability of this novel inhibitor chemotype.

Both Pro167 and Asp240 have been observed to interact with β-lactam substrates or covalent inhibitors in complex structures with CTX-M-9. In a recent crystal structure of CTX-M-9 S70G mutant and cefotaxime (PDB ID 3HLW),[11] the amino group on the aminothiazole ring of cefotaxime forms a hydrogen bond with Asp240 while the methoxyimino group nestles comfortably in the subpocket around Pro167. Compared with the apo structure, such interactions cause small shifts in atom positions for residues in this area (e.g., ~0.5 Å for Asp240Cα); a conformational change not observed in complex structures with smaller substrates such as benzylpenicillin. Similar hydrogen bonds with Asp240 have also been found in previous complex structures with boronic acid inhibitors.[11,12] Additionally, Pro167 and Asp240 are conserved in other CTX-M type enzymes such as Toho-1.[35−37] In the acyl-enzyme complex structure of Toho-1 Glu166A mutant with cefotaxime (PDB ID, 1IYO),[37] the aminothiazole ring makes both a direct and a water-mediated hydrogen bond with Asp240 while establishing vdw interactions with Pro167. Together with our studies described herein, these observations suggest both Asp240 and Pro167 are binding hot spots useful for inhibitor design against CTX-M β-lactamases.

Even more significantly, it is possible to consider targeting similar hot spots in other class A β-lactamases. In narrow-spectrum β-lactamases, such as TEM-1 and SHV-2, residue 240 is a glutamate. Although it has been hypothesized that the substitution of Glu240 for Asp may enlarge the active site and allow ESBLs, such as CTX-M, to accommodate the bulkier side chains of cefotaxime and other third-generation cephalosporins, both Glu240 and Asp240 present similar features in the protein binding pocket, including the net negative charge and the nearly identical positioning of one oxygen atom from the carboxylate group. Comparing the complex structures between a ceftazidime-like boronic acid inhibitor and CTX-M-9 (PDB ID, 1YLY) to that of the same compound with TEM-1 (PDB ID 1M40) shows that the aminothiazole ring of the inhibitor is placed in similar positions and forms a hydrogen bond with residue 240 in both structures.[12,38] Additionally, comparing the affinity of compound **19** with those of compounds **21** and **22** suggests that interactions with the main chain atoms around Gly238, the residue immediately preceding Asp240 (note the numbering gap due to convention), may also contribute significantly to binding. Gly238 is highly conserved in CTX-M, TEM, and SHV enzymes. Meanwhile, the nonpolar binding surface around residue 167 is also largely conserved in these β-lactamases. Like CTX-M, TEM-1 has a proline in this position. Although it is replaced by a threonine in SHV enzymes, most of the carbon atoms, like Cα and Cβ atoms of residues 167 and 168, are in similar positions and thus form a binding subpocket with features comparable to that in CTX-M, albeit with some new features such as Thr167Oγ. In the crystal structure between cefoperazone transition state analog and SHV-1, the carbon atoms of the compound's piperazine ring are in vdw contacts with the Cβ and C atoms of Thr167.[39]

In addition to revealing the importance of Pro167 and Asp240 in ligand binding, the rapid evolution of compound **1** into nanomolar inhibitors like **19** demonstrates the tractability of the tetrazole chemotype as a lead scaffold. The five-member tetrazole ring displays both good shape and electrostatic complementarity with a subpocket usually occupied by the C(3)4′ carboxylate group of β-lactam compounds, forming three hydrogen bonds with Ser130, Thr235, and Ser237 while being stacked against the peptide bond between Thr235 and

Gly236. Several key features of this binding subpocket are also present in the active site of AmpC class C β-lactamase. For example, Thr235 and Gly236 are conserved in AmpC (Thr316 and Gly317). Tyr150, a key catalytic residue in AmpC, places its hydroxyl group in a position similar to that of Ser130 in CTX-M. Other common features shared by the active sites of class A and C enzymes may further allow the design of inhibitors with broader spectra. For instance, existing covalent inhibitors against both classes of enzymes almost invariantly place an oxygen atom in the oxyanion hole formed by two backbone amide groups. A water molecule occupies the oxyanion hole in the complex structures of our tetrazole-based inhibitors. The identification of tetrazole-based inhibitors that favorably displace this water molecule may improve binding affinity and expand the utility of this chemotype to target a wider range of β-lactamases.

CONCLUSIONS

Structurally guided optimization of a novel-class of CTX-M β-lactamase inhibitors has confirmed two binding hot spots that can be targeted to produce high affinity inhibitors. Importantly, these hot spots are shared by other therapeutically important groups of β-lactamases, suggesting the potential for tetrazole-class inhibitors with an expanded spectrum of β-lactamase activity. More generally, the approach we have employed to identify and optimize novel noncovalent inhibitors of CTX-M can be applied to develop novel inhibitors of other important β-lactamases. The nanomolar potency of **19** distinguishes this compound as the highest affinity noncovalent inhibitor yet identified for a class A β-lactamase. Its antimicrobial activity also demonstrates the possible utility of the tetrazole scaffold in countering bacterial resistance. Current efforts are focused on further elaborating the tetrazole chemotype, with the goal of producing a novel class of compounds effective against a wide range of clinically relevant β-lactamases.

EXPERIMENTAL METHODS

Compound Docking. Molecular docking was used as previously described[25] to evaluate newly designed compounds or existing ones from the ZINC small-molecule database with the program DOCK 3.5.54.[25,30−32]

Synthesis. *General Methods.* ^{1}H NMR spectra were recorded on a Varian INOVA-400 400 MHz spectrometer. Chemical shifts are reported in δ units (ppm) relative to TMS as an internal standard. Coupling constants (*J*) are reported in hertz (Hz). The known compounds **1**, **2**, **3**, **4**, **6**, **8**, **10**, and **13**[40] were prepared according the general procedures and/or were obtained from commercial sources (Ryan Scientific, TimTec). All other reagents and solvents were purchased from Aldrich Chemical, Acros Organics, Enamine, Alfa Aesar, and Apollo Scientific and used as received. Air and/or moisture sensitive reactions were carried out under an argon atmosphere in oven-dried glassware using anhydrous solvents from commercial suppliers. Air and/or moisture sensitive reagents were transferred via syringe or cannula and were introduced into reaction vessels through rubber septa. Solvent removal was accomplished with a rotary evaporator at ca. 10−50 Torr. Column chromatography was carried out using a Biotage SP1 flash chromatography system and silica gel cartridges from Biotage. Analytical TLC plates from EM Science (Silica Gel 60 F254) were employed for TLC analyses. Microwave heating was accomplished using a CEM reaction microwave. Hydrogenation reactions were carried out with a ThalesNano H-Cube hydrogenator.

All synthesized analogues tested against CTX-M were judged to be of 95% or higher purity based on analytical LC/MS analysis. LC/MS analyses were performed on a Waters Micromass ZQ/Waters 2795 separation module/Waters 2996 photodiode array detector system controlled by MassLynx 4.0 software. Separations were carried out on an XTerra MS C_{18} 5 μm 4.6 mm × 50 mm column at ambient temperature using a mobile phase of water−acetonitrile containing 0.05% trifluoroacetic acid. Gradient elution was employed wherein the acetonitrile−water ratio was increased linearly from 5% to 95% acetonitrile over 2.5 min, then maintained at 95% acetonitrile for 1.5 min, and then decreased to 5% acetonitrile over 0.5 min and maintained at 5% acetonitrile for 0.5 min. Compound purity was determined by integrating peak areas of the liquid chromatogram, monitored at 254 nm.

General Procedure A. An oven-dried vial or flask is charged with 3-(1*H*-tetrazol-5-yl)aniline (1 equiv), the appropriate carboxylic acid (1 equiv), 1-ethyl-3-[3-dimethylaminopropyl]carbodiimide hydrochloride (1.5 equiv), 1-hydroxybenzotriazole (1.5 equiv), and *N*,*N*′-diisopropylethylamine (2 equiv) and stirred in DMF (0.5 mL) at room temperature for 24 h or until judged complete by LC/MS analysis. The reaction mixture is diluted with water (2 mL), and after adjusting the pH to ∼2 with 1N HCl, the mixture is extracted with ethyl acetate. The organic extracts are washed with brine, dried over magnesium sulfate, and concentrated under reduced pressure. The crude material thus obtained is purified by reverse phase HPLC to afford the desired product.

General Procedure B. An oven-dried vial or flask is charged with 3-(1*H*-tetrazol-5-yl)aniline (1 equiv), the appropriate acid chloride (1.05 equiv), and *N*,*N*′-diisopropylethylamine (2 equiv) and stirred in dichloromethane (5 mL) at room temperature for 30 min. The reaction mixture is diluted with dichloromethane and washed with water. After adjusting the pH to ∼2 with 1N HCl, the mixture is extracted with ethyl acetate. The organic extracts are washed with brine, dried over magnesium sulfate, and concentrated under reduced pressure. The crude material thus obtained is purified by flash column chromatography (5−20% methanol/dichloromethane).

*3-Cyclopropyl-N-[3-(1H-tetrazol-5-yl)-phenyl]-benzamide (**5**).* 3-(1*H*-Tetrazol-5-yl)aniline was reacted with commercially available 3-cyclopropylbenzoic acid according to general procedure A to afford the title compound in 63% yield. ^{1}H NMR (DMSO-d_6) δ 10.42 (s, 1H), 8.55 (s, 1H), 7.93 (d, *J* = 8 Hz, 1H), 7.72 (d, *J* = 8 Hz, 2H), 7.65 (s, 1H), 7.56 (t, *J* = 8 Hz, 1H), 7.39 (t, *J* = 8 Hz, 1H), 7.29 (d, *J* = 8 Hz, 1H), 1.97−2.03 (m, 1H), 0.97−1.01 (m, 2H), 0.74−0.78 (m, 2H). LCMS (ESI) *m*/*z* 306 (MH+).

*3-Acetyl-N-[3-(1H-tetrazol-5-yl)-phenyl]-benzamide (**7**).* 3-(1*H*-Tetrazol-5-yl)aniline was reacted with commercially available 3-acetylbenzoic acid according to general procedure A to afford the title compound in 33% yield. ^{1}H NMR (DMSO-d_6) δ 10.67 (s, 1H), 8.57 (s, 1H), 8.52 (s, 1H), 8.22 (d, *J* = 8 Hz, 1H), 8.16 (d, *J* = 8 Hz, 1H) 7.96 (d, *J* = 8 Hz, 1H), 7.75 (d, *J* = 8 Hz, 1H), 7.70 (t, *J* = 8 Hz, 1H), 7.59 (t, *J* = 8 Hz, 1H), 2.65 (s, 3H). LCMS (ESI) *m*/*z* 308 (MH +).

*N-[3-(1H-Tetrazol-5-yl)-phenyl]-isophthalamic Acid Methyl Ester (**9**).* 3-(1*H*-Tetrazol-5-yl)aniline was reacted with commercially available *mono*-methylisophthalate according to general procedure A to afford the title compound in 22% yield. ^{1}H NMR (DMSO-d_6) δ 10.70 (s, 1H), 8.56 (s, 2H), 8.25 (d, *J* = 8 Hz, 1H), 8.16 (d, *J* = 8 Hz, 1H) 7.96 (d, *J* = 8 Hz, 1H), 7.68−7.75 (m, 2H), 7.58 (t, *J* = 8 Hz, 1H), 3.90 (s, 3H). LCMS (ESI) *m*/*z* 324 (MH+).

*3-Pyrimidin-2-yl-N-[3-(1H-tetrazol-5-yl)-phenyl]-benzamide (**11**).* 3-(1*H*-Tetrazol-5-yl)aniline was reacted with commercially available 3-pyrimidin-2-yl-benzoic acid according to general procedure A to afford the title compound in 11% yield. ^{1}H NMR (DMSO-d_6) δ 10.71 (s, 1H), 8.99 (s, 1H), 8.96 (d, *J* = 4 Hz, 2H), 8.58−8.61 (m, 2H), 8.14 (d, *J* = 8 Hz, 1H), 7.99 (d, *J* = 8 Hz, 1H), 7.68−7.76 (m, 2H), 7.58 (t, *J* = 8 Hz, 1H), 7.49 (d, *J* = 4 Hz, 1H). ^{13}C NMR (100 MHz, DMSO-d_6) δ 166.2, 163.3, 158.5, 140.7, 138.1, 135.9, 131.4, 130.7, 130.4, 129.6, 127.7, 123.6, 122.8, 121.0, 119.3. LCMS (ESI) *m*/*z* 344 (MH+).

*3-Dimethylaminomethyl-N-[3-(1H-tetrazol-5-yl)-phenyl]-benzamide (**12**).* 3-(1*H*-Tetrazol-5-yl)aniline was reacted with commercially

dx.doi.org/10.1021/jm2014138 | J. Med. Chem. 2012, 55, 2163−2172

available 3-dimethylaminomethyl-benzoic acid according to general procedure A to afford the title compound in 28% yield. ^{1}H NMR (DMSO-d_6) δ 10.60 (s, 1H), 8.57 (s, 1H), 8.08−8.10 (m, 2H), 7.95 (d, J = 8 Hz, 1H), 7.70−7.76 (m, 2H), 7.58−7.64 (m, 2H), 4.37 (s, 2H), 2.75 (s, 6H). ^{13}C NMR (100 MHz, DMSO-d_6) δ 165.9, 140.5, 135.9, 134.8, 131.4, 131.3, 130.5, 129.7, 129.3, 123.5, 122.9, 119.4, 60.0, 42.5. LCMS (ESI) m/z 323 (MH+)

*3-Cyano-N-[3-(1H-tetrazol-5-yl)-phenyl]-benzamide (**14**).* 3-(1*H*-Tetrazol-5-yl)aniline was reacted with commercially available 3-cyanobenzoic acid according to general procedure A and purified by flash column chromatography (5−15% methanol/dichloromethane) to afford the title compound in 66% yield. ^{1}H NMR (DMSO-d_6) δ 10.63 (s, 1H), 8.53 (s, 1H), 8.43 (s, 1H), 8.25 (d, J = 8 Hz, 1H), 8.06 (d, J = 8 Hz, 1H) 7.92 (d, J = 8 Hz, 1H), 7.75 (d, J = 8 Hz, 2H), 7.56 (t, J = 8 Hz, 1H). LCMS (ESI) m/z 291 (MH+).

*1H-Indole-4-carboxylic Acid [3-(1H-Tetrazol-5-yl)-phenyl]-amide (**15**).* 3-(1*H*-Tetrazol-5-yl)aniline was reacted with commercially available indole-4-carboxylic acid according to general procedure A to afford the title compound in 10% yield. ^{1}H NMR (DMSO-d_6) δ 11.35 (s, 1H), 10.41 (s, 1H), 8.65 (s, 1H), 7.93 (d, J = 8 Hz, 1H), 7.70 (d, J = 4 Hz, 1H), 7.53−7.62 (m, 3H), 7.47 (s, 1H), 7.20 (t, J = 8 Hz, 1H), 6.85 (s, 1H). LCMS (ESI) m/z 305 (MH+).

*3H-Benzoimidazole-4-carboxylic Acid [3-(1H-Tetrazol-5-yl)-phenyl]-amide (**16**).* 3-(1*H*-Tetrazol-5-yl)aniline (75 mg, 0.47 mmol), 1*H*-benzimidazole-4-carboxylic acid (76 mg, 0.47 mmol), 1-ethyl-3-[3-dimethylaminopropyl]carbodiimide hydrochloride (135 mg, 0.7 mmol), 1-hydroxybenzotriazole (95 mg, 0.7 mmol), and *N*,*N*′-diisopropylethylamine (0.17 mL, 0.94 mmol) were stirred in DMF (0.5 mL) at room temperature for 4 h. The reaction mixture was diluted with water (1 mL), and after adjusting the pH to ∼4 with 1N HCl, the mixture was filtered. The filtered precipitate was purified by reverse phase HPLC to afford the product as a trifluoroacetic acid salt in 21% yield. ^{1}H NMR (DMSO-d_6) δ 11.69 (s, 1H), 9.00 (s, 1H), 8.61 (s, 1H), 8.12 (d, J = 8 Hz, 1H), 7.93−7.99 (m, 2H), 7.79 (d, J = 8 Hz, 1H), 7.52−7.63 (m, 2H). ^{13}C NMR (100 MHz, DMSO-d_6) δ 164.1, 159.2, 148.4, 143.4, 140.2, 134.3, 130.8, 125.6, 124.3, 123.1, 122.9, 121.9, 118.9, 118.4. LCMS (ESI) m/z 306 (MH+).

*1H-Indole-5-carboxylic Acid [3-(1H-Tetrazol-5-yl)-phenyl]-amide (**17**).* 3-(1*H*-Tetrazol-5-yl)aniline was reacted with commercially available indole-5-carboxylic acid according to the general procedure A to afford the title compound in 9% yield. ^{1}H NMR (DMSO-d_6) δ 11.39 (s, 1H), 10.36 (s, 1H), 8.62 (s, 1H), 8.30 (s, 1H), 7.96 (d, J = 8 Hz, 1H), 7.75 (d, J = 8 Hz, 1H), 7.69 (d, J = 8 Hz, 1H), 7.45−7.57 (m, 3H), 6.58 (s, 1H). LCMS (ESI) m/z 305 (MH+).

*1H-Indazole-5-carboxylic Acid [3-(1H-Tetrazol-5-yl)-phenyl]-amide (**18**).* 3-(1*H*-Tetrazol-5-yl)aniline was reacted with commercially available indazole-5-carboxylic acid according to general procedure A to afford the title compound in 6% yield. ^{1}H NMR (DMSO-d_6) δ 10.50 (s, 1H), 8.61 (s, 1H), 8.51 (s, 1H), 8.26 (s, 1H), 7.95−7.98 (m, 3H), 7.71 (d, J = 4 Hz, 1H), 7.64 (d, J = 8 Hz, 1H), 7.57 (t, J = 8 Hz, 1H). LCMS (ESI) m/z 306 (MH+).

*6-Trifluoromethyl-3H-benzoimidazole-4-carboxylic Acid [3-(1H-Tetrazol-5-yl)-phenyl]-amide (**19**).* 3-(1*H*-Tetrazol-5-yl)aniline (15 mg, 0.09 mmol), 6-trifluoromethyl-benzimidazole-4-carboxylic acid (25 mg, 0.09 mmol), 1-ethyl-3-[3-dimethylaminopropyl]carbodiimide hydrochloride (26 mg, 0.135 mmol), 1-hydroxybenzotriazole (18 mg, 0.135 mmol), and *N*,*N*′-diisopropylethylamine (0.047 mL, 0.27 mmol) were stirred in DMF (0.2 mL) at room temperature for 24 h. The reaction mixture was filtered and purified by reverse phase HPLC to afford the title compound as a trifluoroacetic acid salt in 30% yield. ^{1}H NMR (DMSO-d_6) δ 8.78 (s, 1H), 8.54 (s, 1H), 8.24 (d, J = 12 Hz, 2H), 8.02 (d, J = 8 Hz, 1H), 7.80 (d, J = 8 Hz, 1H), 7.64 (t, J = 8 Hz, 1H). ^{13}C NMR (100 MHz, DMSO-d_6) δ 163.1, 155.1, 146.9, 140.0, 130.9, 126.5, 125.6, 123.8, 123.5, 123.1, 122.3, 119.6, 118.8, 94.6. LCMS (ESI) m/z 374 (MH+).

*3-Bromo-5-hydroxy-N-[3-(1H-tetrazol-5-yl)-phenyl]-benzamide (**20**).* 3-(1*H*-Tetrazol-5-yl)aniline was reacted with commercially available 3-bromo-5-hydroxybenzoic acid according to general procedure A to afford the title compound in 22% yield. ^{1}H NMR (DMSO-d_6) δ 10.48 (s, 1H), 10.27 (s, 1H), 8.55 (s, 1H), 7.91 (d, J = 8 Hz, 1H), 7.72 (d, J = 4 Hz, 1H), 7.60 (s, 1H), 7.56 (d, J = 8 Hz, 1H), 7.34 (s, 1H), 7.15 (s, 1H). LCMS (ESI) m/z 361 (MH+).

*3-Hydroxy-N-[3-(1H-tetrazol-5-yl)-phenyl]-5-trifluoromethyl-benzamide (**21**).* 3-(1*H*-Tetrazol-5-yl)aniline was reacted with commercially available 3-hydroxy-5-trifluoromethyl carboxylic acid according to general procedure A to afford the title compound in 24% yield. ^{1}H NMR (DMSO-d_6) δ 10.60 (s, 1H), 10.51 (s, 1H), 8.55 (s, 1H), 7.94 (d, J = 8 Hz, 1H), 7.74 (d, J = 12 Hz, 2H), 7.64 (s, 1H), 7.58 (d, J = 8 Hz, 1H), 7.24 (s, 1H). LCMS (ESI) m/z 350 (MH+).

*3-Amino-N-[3-(1H-tetrazol-5-yl)-phenyl]-5-trifluoromethyl-benzamide (**22**).* 3-(1*H*-Tetrazol-5-yl)aniline (75 mg, 0.47 mmol), 3-amino-5-trifluoromethyl-benzoic acid (96 mg, 0.47 mmol), 1-ethyl-3-[3-dimethylaminopropyl]carbodiimide hydrochloride (135 mg, 0.7 mmol), 1-hydroxybenzotriazole (95 mg, 0.7 mmol), and *N*,*N*′-diisopropylethylamine (0.16 mL, 0.94 mmol) were stirred in DMF (0.5 mL) at room temperature for 18 h. The reaction mixture was filtered and purified by reverse phase HPLC to afford the title compound in 52% yield. ^{1}H NMR (DMSO-d_6) δ 10.50 (s, 1H), 8.53 (s, 1H), 7.92 (d, J = 8 Hz, 1H), 7.72 (d, J = 8 Hz, 1H), 7.56 (t, J = 8 Hz, 1H), 7.37 (d, J = 8 Hz, 2H), 7.24 (s, 1H). LCMS (ESI) m/z 349 (MH+).

*6-Fluoro-3H-benzoimidazole-4-carboxylic Acid [3-(1H-Tetrazol-5-yl)-phenyl]-amide (**23**).* 3-(1*H*-Tetrazol-5-yl)aniline was reacted with commercially available 6-fluoro-benzimidazole-4-carboxylic acid according to the general procedure A to afford the title compound in 17% yield. ^{1}H NMR (DMSO-d_6) δ 8.63 (s, 1H), 8.53 (s, 1H), 7.99 (d, J = 8 Hz, 1H), 7.71−7.80 (m, 4H), 7.63 (t, J = 8 Hz, 1H). LCMS (ESI) m/z 324 (MH+).

*3-Bromo-5-cyano-N-[3-(1H-tetrazol-5-yl)-phenyl]-benzamide (**24**).* 3-(1*H*-Tetrazol-5-yl)aniline was reacted with commercially available 3-cyano-5-bromobenzoic acid according to the general procedure A to afford the title compound in 24% yield. ^{1}H NMR (DMSO-d_6) δ 10.70 (s, 1H), 8.53 (s, 1H), 8.45 (s, 1H), 8.41 (d, J = 8 Hz, 2H), 7.94 (d, J = 8 Hz, 1H), 7.76 (d, J = 8 Hz, 1H), 7.59 (t, J = 8 Hz, 1H). LCMS (ESI) m/z 370 (MH+).

*2-Amino 3-Nitro-5-trifluoromethylbenzoic Acid (**25**).* Commercially available 2-chloro-3-nitro-5-trifluoromethylbenzoic acid (0.10 g, 0.37 mmol) and aqueous ammonium hydroxide (2 mL) were heated in a sealed tube in a CEM microwave at 120 °C for an hour. After cooling, the pH was adjusted to 2 with 1N HCl. The precipitate was filtered and dried to obtain 2-amino 3-nitro-5-trifluoromethylbenzoic acid as a yellow solid (80 mg). This material was used in the next step without further purification. ^{1}H NMR (DMSO-d_6) δ 8.49 (s, 1H), 8.32 (s, 1H).

*2,3-Diamino-5-trifluoromethylbenzoic Acid (**26**).* A solution of 2-amino-3-nitro-5-trifluoromethylbenzoic acid (**25**, 75 mg, 0.3 mmol) in methanol was passed through a Pd/C cartridge (10 wt %) at a flow rate of 1 mL/min using the H-Cube hydrogenation system. The solution was concentrated under reduced pressure and dried to obtain the title compound (62 mg). This material was used without further purification in the next reaction. ^{1}H NMR ($CDCl_3$) δ 7.80 (s, 1H), 7.05 (s, 1H). LCMS (ESI) m/z 221 (MH+).

*6-Trifluoromethyl-benzimidazole-4-carboxylic Acid (**27**).* Formic acid (0.34 mmol, 3 equiv) was added to intermediate **26** (0.11 mmol, 1 equiv) in aqueous 4 M HCl (0.35 mL) and the reaction mixture heated to 100 °C for 2 h. The reaction mixture was concentrated under reduced pressure and dried to obtain the title compound (35 mg) as a hydrochloride salt. This material was used without further purification in the next reaction. ^{1}H NMR (DMSO-d_6) δ 8.74 (s, 1H), 8.33 (s, 1H), 8.07 (s, 1H). LCMS (ESI) m/z 231 (MH+).

Protein Purification, Crystallization and Structure Determination. CTX-M-9, a class A β-lactamase that we have previously studied, was used to represent the CTX-M family. The protein was purified as previously described[10] and crystallized in 1.2−1.6 M potassium phosphate buffer (pH 8.3) from hanging drops at 20 °C. The final concentration of the protein in the drop ranged from 6.5 mg mL^{-1} to 9 mg mL^{-1}. The complex crystals were obtained through soaking methods. On the basis of the variability in terms of solubility and affinity, compound soaking times varied considerably, from 1 to 24 h. Diffraction was measured at two beamlines: X6A at National

Synchrotron Light Source, Brookhaven, New York, and 23-ID-B of GM/CA CAT at Advanced Photon Source (APS), Argonne, Illinois. Data were processed with HKL2000.[41] The models for refinement were first obtained through using a rigid-body refinement by Refmac in CCP4[42] with an apo CTX-M-9 structure. CCP4 and Coot[43] were used to complete the model rebuilding and refinement.

Inhibition Assays. The hydrolysis reaction of CTX-M activity was measured using the β-lactam substrate nitrocefin in 100 mM Tris-HCl (pH 7.0, with 0.01% v/v Triton X-100) and monitored using a Biotek Synergy Mx monochromator-based multimode microplate reader at 480 nM wavelength. Nitrocefin was 50 μM in the inhibition assays. The K_m of nitrocefin for CTX-M was determined to be 24 μM. The compounds were synthesized as previously described or purchased from the company Chembridge and assayed without further purification. The highest concentrations at which the compounds were tested were up to 1−3 mM (depending on their solubility) in the IC_{50} experiment. The reaction was initiated by adding protein to the reaction buffer last.

Microbiology. Susceptibility testing was performed and interpreted following the guidelines of CLSI.[34] The compounds were dissolved in DMSO, and dilutions were performed using Muller−Hinton medium. An adequate final concentration was obtained to determine the minimum inhibitory concentrations (MICs). The concentration of DMSO was maintained below 10%. The inhibitors were tested for synergy with the third-generation β-lactam cefotaxime against two clinical bacteria. The ratio of β-lactam to inhibitor was 1:1. Each value reported reflects the average of three independent experiments. The bacteria belonged to the species *Escherichia coli* and exhibited high level of resistance to β-lactams because of CTX-M-9 and CTX-M-14 β-lactamases. For disk diffusion plate assays, bacterial strains were diluted in sterile water to a turbidity equivalent to 0.5 McFarland turbidity standards. After a subsequent 10-fold dilution, the bacterial suspensions were inoculated on Mueller Hinton agar. The plates were dried for 10 min before applying the disks containing cefotaxime antibiotic (30 μg) or the inhibitor (30 μg) or both (cefotaxime:inhibitor: 30 μg:15 μg, 30 μg:30 μg) or the solvent. After overnight incubation at 37 °C, the zones of bacterial-growth inhibition were measured.

■ ASSOCIATED CONTENT

Accession Codes

The coordinates and structure factors have been deposited in the Protein Data Bank with the accession codes 4DE3, 4DDY, 4DDS, 4DE2, 4DE0, and 4DE1 for CTX-M-9 in complex with **4**, **10**, **11**, **12**, **16**, and **18**, respectively.

■ AUTHOR INFORMATION

Corresponding Author

*For A.R.R.: phone, (415) 514-9698; fax, (415) 482-1972; E-mail, adam.renslo@ucsf.edu. For Y.C.: phone, (813) 974-7809; fax, (813) 974-7357; E-mail, ychen1@health.usf.edu.

Present Addresses

[‖]Diablo Valley College, Department of Chemistry, Pleasant Hill, California 94523, United States.

[⊥]Lebanese University, EDST, AZM Center for Biotechnology Research and Applications, Tripoli, Lebanon.

Notes

The authors declare no competing financial interest.

■ ACKNOWLEDGMENTS

We thank Dr. Rongshi Li for insightful discussions and Eric Lewandowski for reading the manuscript. This work was supported by USF Start-up Fund (to Y.C.) and the Sandler Foundation (to A.R.R.).

■ ABBREVIATIONS USED

ESBL, extended spectrum β-lactamase; CTX-M, cefotaximase; GPCR, G-protein coupled receptor; HTS, high-throughput screening; vdw, van der Waals

■ REFERENCES

(1) Chen, Y.; Zhang, W.; Shi, Q.; Hesek, D.; Lee, M.; Mobashery, S.; Shoichet, B. K. Crystal structures of penicillin-binding protein 6 from *Escherichia coli*. *J. Am. Chem. Soc.* **2009**, *131*, 14345−14354.

(2) Llarrull, L. I.; Testero, S. A.; Fisher, J. F.; Mobashery, S. The future of the beta-lactams. *Curr. Opin. Microbiol.* **2010**, *13*, 551−557.

(3) Tipper, D. J.; Strominger, J. L. Mechanism of action of penicillins: a proposal based on their structural similarity to acyl-D-alanyl-D-alanine. *Proc. Natl. Acad. Sci. U.S.A.* **1965**, *54*, 1133−1141.

(4) Silvaggi, N. R.; Anderson, J. W.; Brinsmade, S. R.; Pratt, R. F.; Kelly, J. A. The crystal structure of phosphonate-inhibited D-Ala-D-Ala peptidase reveals an analogue of a tetrahedral transition state. *Biochemistry* **2003**, *42*, 1199−1208.

(5) Frere, J. M. Beta-lactamases and bacterial resistance to antibiotics. *Mol. Microbiol.* **1995**, *16*, 385−395.

(6) Fisher, J. F.; Meroueh, S. O.; Mobashery, S. Bacterial resistance to beta-lactam antibiotics: compelling opportunism, compelling opportunity. *Chem. Rev.* **2005**, *105*, 395−424.

(7) Taubes, G. The bacteria fight back. *Science* **2008**, *321*, 356−361.

(8) Bush, K.; Jacoby, G. A.; Medeiros, A. A. A functional classification scheme for beta-lactamases and its correlation with molecular structure. *Antimicrob. Agents Chemother.* **1995**, *39*, 1211−1233.

(9) Livermore, D. M. beta-Lactamases in laboratory and clinical resistance. *Clin. Microbiol. Rev.* **1995**, *8*, 557−584.

(10) Chen, Y.; Delmas, J.; Sirot, J.; Shoichet, B.; Bonnet, R. Atomic resolution structures of CTX-M beta-lactamases: extended spectrum activities from increased mobility and decreased stability. *J. Mol. Biol.* **2005**, *348*, 349−362.

(11) Delmas, J.; Leyssene, D.; Dubois, D.; Birck, C.; Vazeille, E.; Robin, F.; Bonnet, R. Structural insights into substrate recognition and product expulsion in CTX-M enzymes. *J. Mol. Biol.* **2010**, *400*, 108−120.

(12) Chen, Y.; Shoichet, B.; Bonnet, R. Structure, function, and inhibition along the reaction coordinate of CTX-M beta-lactamases. *J. Am. Chem. Soc.* **2005**, *127*, 5423−5434.

(13) Bonnet, R. Growing group of extended-spectrum beta-lactamases: the CTX-M enzymes. *Antimicrob. Agents Chemother.* **2004**, *48*, 1−14.

(14) Bradford, P. A. Extended-spectrum beta-lactamases in the 21st century: characterization, epidemiology, and detection of this important resistance threat. *Clin. Microbiol. Rev.* **2001**, *14*, 933−951.

(15) Drawz, S. M.; Bonomo, R. A. Three decades of beta-lactamase inhibitors. *Clin. Microbiol. Rev.* **2010**, *23*, 160−201.

(16) Bennett, P. M.; Chopra, I. Molecular basis of beta-lactamase induction in bacteria. *Antimicrob. Agents Chemother.* **1993**, *37*, 153−158.

(17) Jacobs, C.; Frere, J. M.; Normark, S. Cytosolic intermediates for cell wall biosynthesis and degradation control inducible beta-lactam resistance in gram-negative bacteria. *Cell* **1997**, *88*, 823−832.

(18) Petrosino, J.; Cantu, C. III; Palzkill, T. beta-Lactamases: protein evolution in real time. *Trends Microbiol.* **1998**, *6*, 323−327.

(19) Pages, J. M.; Lavigne, J. P.; Leflon-Guibout, V.; Marcon, E.; Bert, F.; Noussair, L.; Nicolas-Chanoine, M. H. Efflux pump, the masked side of beta-lactam resistance in *Klebsiella pneumoniae* clinical isolates. *PLoS ONE* **2009**, *4*, e4817.

(20) Bonnefoy, A.; Dupuis-Hamelin, C.; Steier, V.; Delachaume, C.; Seys, C.; Stachyra, T.; Fairley, M.; Guitton, M.; Lampilas, M. In vitro activity of AVE1330A, an innovative broad-spectrum non-beta-lactam beta-lactamase inhibitor. *J. Antimicrob. Chemother.* **2004**, *54*, 410−417.

(21) Majumdar, S.; Pratt, R. F. Inhibition of class A and C beta-lactamases by diaroyl phosphates. *Biochemistry* **2009**, *48*, 8285−8292.

(22) Morandi, F.; Caselli, E.; Morandi, S.; Focia, P. J.; Blazquez, J.; Shoichet, B. K.; Prati, F. Nanomolar inhibitors of AmpC beta-lactamase. *J. Am. Chem. Soc.* **2003**, *125*, 685−695.
(23) Strynadka, N. C.; Martin, R.; Jensen, S. E.; Gold, M.; Jones, J. B. Structure-based design of a potent transition state analogue for TEM-1 beta-lactamase. *Nature Struct. Biol.* **1996**, *3*, 688−695.
(24) Tondi, D.; Morandi, F.; Bonnet, R.; Costi, M. P.; Shoichet, B. K. Structure-based optimization of a non-beta-lactam lead results in inhibitors that do not up-regulate beta-lactamase expression in cell culture. *J. Am. Chem. Soc.* **2005**, *127*, 4632−4639.
(25) Chen, Y.; Shoichet, B. K. Molecular docking and ligand specificity in fragment-based inhibitor discovery. *Nature Chem. Biol.* **2009**, *5*, 358−364.
(26) Chen, Y.; Pohlhaus, D. T. In silico docking and scoring of fragments. *Drug Discovery Today: Technol.* **2010**, *7*, 149−156.
(27) Hert, J.; Irwin, J. J.; Laggner, C.; Keiser, M. J.; Shoichet, B. K. Quantifying biogenic bias in screening libraries. *Nature Chem. Biol.* **2009**, *5*, 479−483.
(28) O'Shea, R.; Moser, H. E. Physicochemical properties of antibacterial compounds: implications for drug discovery. *J. Med. Chem.* **2008**, *51*, 2871−2878.
(29) Payne, D. J.; Gwynn, M. N.; Holmes, D. J.; Pompliano, D. L. Drugs for bad bugs: confronting the challenges of antibacterial discovery. *Nature Rev. Drug Discovery* **2007**, *6*, 29−40.
(30) Chen, Y.; Bonnet, R.; Shoichet, B. K. The acylation mechanism of CTX-M beta-lactamase at 0.88 a resolution. *J. Am. Chem. Soc.* **2007**, *129*, 5378−5380.
(31) Lorber, D. M.; Shoichet, B. K. Hierarchical docking of databases of multiple ligand conformations. *Curr. Top. Med. Chem.* **2005**, *5*, 739−749.
(32) Irwin, J. J.; Shoichet, B. K. ZINC—a free database of commercially available compounds for virtual screening. *J. Chem. Inf. Model.* **2005**, *45*, 177−182.
(33) Ryckmans, T.; Edwards, M. P.; Horne, V. A.; Correia, A. M.; Owen, D. R.; Thompson, L. R.; Tran, I.; Tutt, M. F.; Young, T. Rapid assessment of a novel series of selective CB2 agonists using parallel synthesis protocols: a lipophilic efficiency (LipE) analysis. *Bioorg. Med. Chem. Lett.* **2009**, *19*, 4406−4409.
(34) Wayne, P. Performance Standards for Antimicrobial Susceptibility Testing; 20th Informational Supplement. *Clin. Lab. Stand. Inst.* **2010**, *M100−S20*, 1−23.
(35) Ibuka, A. S.; Ishii, Y.; Galleni, M.; Ishiguro, M.; Yamaguchi, K.; Frere, J. M.; Matsuzawa, H.; Sakai, H. Crystal structure of extended-spectrum beta-lactamase Toho-1: insights into the molecular mechanism for catalytic reaction and substrate specificity expansion. *Biochemistry* **2003**, *42*, 10634−10643.
(36) Tomanicek, S. J.; Blakeley, M. P.; Cooper, J.; Chen, Y.; Afonine, P. V.; Coates, L. Neutron diffraction studies of a class A beta-lactamase Toho-1 E166A/R274N/R276N triple mutant. *J. Mol. Biol.* **2010**, *396*, 1070−1080.
(37) Shimamura, T.; Ibuka, A.; Fushinobu, S.; Wakagi, T.; Ishiguro, M.; Ishii, Y.; Matsuzawa, H. Acyl-intermediate structures of the extended-spectrum class A beta-lactamase, Toho-1, in complex with cefotaxime, cephalothin, and benzylpenicillin. *J. Biol. Chem.* **2002**, *277*, 46601−46608.
(38) Minasov, G.; Wang, X.; Shoichet, B. K. An ultrahigh resolution structure of TEM-1 beta-lactamase suggests a role for Glu166 as the general base in acylation. *J. Am. Chem. Soc.* **2002**, *124*, 5333−5340.
(39) Ke, W.; Sampson, J. M.; Ori, C.; Prati, F.; Drawz, S. M.; Bethel, C. R.; Bonomo, R. A.; van den Akker, F. Novel insights into the mode of inhibition of class A SHV-1 beta-lactamases revealed by boronic acid transition state inhibitors. *Antimicrob. Agents Chemother.* **2011**, *55*, 174−183.
(40) Makovec, F.; Peris, W.; Revel, L.; Giovanetti, R.; Redaelli, D.; Rovati, L. C. Antiallergic and cytoprotective activity of new *N*-phenylbenzamido acid derivatives. *J. Med. Chem.* **1992**, *35*, 3633−3640.
(41) Otwinowski, Z.; Minor, W. Processing of X-ray diffraction data collected in oscillation mode. *Methods Enzymol.* **1997**, *276*, 307−326.
(42) Collaborative Computational Project, N. The CCP4 suite: programs for protein crystallography. *Acta Crystallogr., Sect. D: Biol. Crystallogr.* **1994**, *50*, 760−763.
(43) Emsley, P.; Cowtan, K. Coot: model-building tools for molecular graphics. *Acta Crystallogr., Sect. D: Biol. Crystallogr.* **2004**, *60*, 2126−2132.